Supporting Online Material for

Fluorescence-force spectroscopy maps two-dimensional reaction landscape of the Holliday junction

Sungchul Hohng, Ruobo Zhou, Michelle K. Nahas, Jin Yu, Klaus Schulten, David M. J. Lilley & Taekjip Ha*

*To whom correspondence should be addressed (tjha@uiuc.edu).

This PDF file includes:

Content:

MATERIALS AND METHODS

Sample assembly. Nonspecific binding of the DNA and beads was prevented using cover slips coated with poly-ethylene glycol as previously described(1). The sample chamber was sequentially incubated with (1) neutravidin (0.25 mg/ml) for 10 min, 2) blocking buffer containing tRNA (1 mg/ml) and BSA (1 mg/ml) for 1 h, 3) junction- λ-DNA (50 pM in HJ) for 40 min, 4) a solution of anti-digoxigenin coated bead for 30 min, and 5) imaging buffer comprising 10 mM Tris (pH 8.0), 5 mM NaCl, 10 mM $MgCl_2$, 1 mg/ml BSA, 1mg/ml blocking DNA, 0.04 mg/ml anti-digoxigenin, 0.4 % (w/v) D-glucose (Sigma), 165 U/ml glucose oxidase (Sigma # G2133), 2170 U/ml catalase (Roche # 10106810001), and 1 mM Trolox (Sigma) (2)). Steps 3-5 were carried out using a syringe pump to minimize DNA shearing.

Experimental scheme and data analysis. The tethered position of the trapped bead was determined with an accuracy greater than 100 nm by finding the central position of the stretching curves in two orthogonal directions in the sample plane. The force-extension curves were used to determine the extension required to achieve the desired stretching force. Before collecting the data a more accurate central position of the molecule was determined from the confocal image of single-molecule fluorescence from the HJ displaced 13 μm from the trap center. At different stretching lengths, single-molecule fluorescence signals were collected for 10 s at room temperature with 5 ms (junction *BR*) and 10 ms (all others) time resolution. The measurements were repeated for the same molecule until photobleaching. The confocal beam was programmed to follow the motion the HJ using the mapping generated between the sample scanning and beam scanning. To determine transition rates at different forces, hidden Markov modeling was used as described

previously (3) .

DNA sequences for the three different Holliday junction structures

Junction *XR*

b-strand: 5'-/Cy5/ CCC TAG CAA GCC GCT GCT ACG G-3'

h-strand: 5'-/Cy3/ CCG TAG CAG CGC GAG CGG TGG G-3'

r-strand: 5'-/biotin/ CCC ACC GCT CGG CTC AAC TGG G-3'

x-strand: 5'-GGG CGG CGA CCT CCC AGT TGA GCG CTT GCT AGG G-3'

Junction *XR*-long

b-strand: 5'-/Cy5/ CCC TAG CAA GCC GCT GCT ACG G-3'

h-strand: 5'-/Cy3/ CCG TAG CAG CGC GAG CGG TGG GCG AAC GCT TA-3'

r-strand: 5'-/biotin/ TAA GCG TTC GCC CAC CGC TCG GCT CAA CTG GGA CCG TTT CGT-3'

x-strand: 5'-GGG CGG CGA CCT ACG AAA CGG TCC CAG TTG AGC GCT TGC TAG GG-3'

Junction *HR*

b-strand: 5'-/Cy5/ CCC TAG CAA GCC GCT GCT ACG G /Cy3/-3'

h-strand: 5'-GGG CGG CGA CCT TTT CCG TAG CAG CGC GAG CGG TGG G-3'

r-strand: 5'-/biotin/ CCC ACC GCT CGG CTC AAC TGG G-3'

x-strand: 5'-CCC AGT TGA GCG CTT GCT AGG G-3'

Junction *BR*

b-strand: 5' - /5Phos/GGG CGG CGA CCT CCC TAG CAA GCC GCT GCT ACG G - 3'

h-strand: 5' - /5Cy3/CCG TAG CAG CGC GAG CGG TGG G - 3'

r-strand: 5'-*/biotin/* CCC ACC GCT CGG CTC AAC TGG G-3'

x-strand: 5' - CCC AGT TGA GCG CTT GCT AGG G/3Cy5Sp/ - 3'

Construction of Holliday junction species. DNA strands were purchased from IDTDNA (Coralville, IA). The Holliday junction were annealed as follows. Biotinylated (10 μM) and non-biotinylated strands were mixed in 1:1.2 molar ratio in a buffer containing 10 mM

Tris (pH 8) and 50 mM NaCl. The mixture was cooled on a heating block from 90 ºC to room temperature over the course of 3 ~ 4 hours.

Annealing Holliday junction and λ-DNA. λ-DNA was purchased from New England Biolabs (Ipswich, MA). To separate the cohesive ends of the circular form of λ-DNA into a linear form, the λ-DNA (~ 20 nM) was heated in the presence of 0.5 M NaCl to 87 ºC for 10 minutes and then set on ice for 5 minutes. Rapid cooling prevents the cohesive ends from reannealing. The previously annealed Holliday junction (3 µl, 110 nM) and BSA (1 µl of 20mg/ml) was added to the λ-DNA solution and the mixture was tumbled at room temperature for 90 min, followed by 90 min at 4 ºC. Finally, a DNA oligonucleotdie labeled with digoxigenin that was complementary to a cohesive end of λ-DNA (5'-AGG TCG CCG CCC /digoxigenin/-3', IDTDNA:1 µl, 10 µM) was added and the resulting mixture tumbled at 4 ºC for additional 1 h. After the annealing process, the mixture was diluted by addition of 250 µl 10 mM Tris (pH 8.0), 50 mM NaCl, 0.1 mg/ml BSA. The final sample was frozen at -20 C in 10 µl aliquots.

Preparation of anti-digoxigenin coated beads. Protein G-coated polystyrene beads (1.0 µm, Polysciences) were cross-linked to sheep anti-digoxigenin (Roche Applied Science) following the protocol below provided by Wei Cheng (U.C. Berkeley).

1) Take 0.5 ml of protein G-coated bead and transfer beads into crosslinking buffer (0.1 M Na2HPO4, 0.1 M NaCl) by repeating 3~4 times centrifugation (4 minutes at 7000 rpm), removing supernatant, and adding 0.5 ml of the crosslinking buffer.

2) Add 40 µl of anti-digoxigenin (1mg/ml dissolved in 0.019 M NaH_2PO_4, 0.081 M Na_2HPO_4, 0.14 M NaCl, 2.7 mM KCl) and 15 µl of DMP (50 mg/ml dissolved in the crosslinking buffer) to the tube.

3) Tumble the reaction tube for 2 hours at room temperature.

4) To stop the reaction, add 30 μl of Tris buffer (1M, pH6.8) and continue tumbling for another two hours.

5) Transfer beads into bead storage buffer (0.039 M NaH_2PO_4, 0.061 M Na_2HPO_4, 0.14 M NaCl, 2.7 mM KCl) by repeating 3 ~ 4 times centrifugation (4 minutes at 7000 rpm), removing supernatant, and adding 0.5 ml of the bead storage buffer.

6) Add 5 μl of sodium azide (2 %) to the tube and keep the beads at 4 ºC.

7) For sample assembly, 10~100 times diluted bead in Tris 10mM, pH8.0 buffer was used.

Geometrical model of Holliday junction in angular and Cartesian coordinates

Here, we describe a simplified geometrical model that depicts the HJ conformation using two angular coordinates. Starting from this configuration shown, bend 1 and 2 out of the page by $\psi/2$ each, and 3 and 4 into the page by $\psi/2$ each. Assuming each arm length is 1,

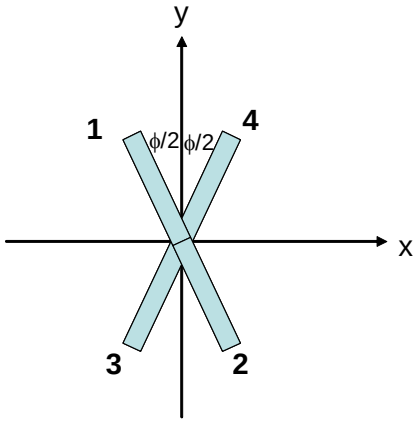

$$\mathbf{1}: \quad \left(-\cos\frac{\psi}{2}\sin\frac{\phi}{2}, \cos\frac{\psi}{2}\cos\frac{\phi}{2}, \sin\frac{\psi}{2}\right)$$

$$\mathbf{2}: \quad \left(\cos\frac{\psi}{2}\sin\frac{\phi}{2}, \cos\frac{\psi}{2}\cos\frac{\phi}{2}, \sin\frac{\psi}{2}\right)$$

$$\mathbf{3}: \quad \left(-\cos\frac{\psi}{2}\sin\frac{\phi}{2}, -\cos\frac{\psi}{2}\cos\frac{\phi}{2}, -\sin\frac{\psi}{2}\right)$$

$$\mathbf{4}: \quad \left(\cos\frac{\psi}{2}\sin\frac{\phi}{2}, \cos\frac{\psi}{2}\cos\frac{\phi}{2}, -\sin\frac{\psi}{2}\right)$$

From these coordinates, we can easily calculate the distance between two ends of any pair of helices. For example, d_{HR}, the distance between the ends of arms H and R, in *iso*I would be given by the distance between points 1 and 4 above multiplied by the effective arm length L_{eff}. Likewise, d_{BR} in *iso*I would be given by the distance between points 1 and 3

above multiplied by L_{eff}. In this model, d_{HR} in *iso*I would be identical to d_{XR} in *iso*II and d_{BR} would be identical in *iso*I and *iso*II. These are good assumptions as long as one strand being pulled is an exchanging strand and the other strand being pulled is a continuous strand which was true for junctions *XR* and *HR*, but not for junction *BR*. In fact, in junction *BR*, d_{BR} is expected to be larger in isoI where both of the pulled strands are the continuous strands (therefore at the outer sides of the HJ for 11 bp long arms) than in *iso*II where both of the pulled strands are the exchanging strands (therefore at the inner sides of the HJ). This expectation is consistent with our observation that *iso*I is favored at higher forces for junction *BR*.

Estimating ϕ and ψ angles at the transition state

Our data presented in the paper is not consistent with a single transition state that is valid regardless of pulling direction. Rather, our data suggest that the configuration of the transition state depends on the pulling direction. A possible explanation for this effect is the existence of two transition states of equivalent free energy, each belonging to the angular coordinate space defined by the stacking configurations, I and II. In such a model, applying tension in the direction that favors isoII (as in junction *HR*) will lower the free energy of the transition state belonging to $(\phi_{\text{II}}, \psi_{\text{II}})$ space, termed *ts*II, relative to that of the transition state belonging to $(\phi_{\text{I}}, \psi_{\text{I}})$ space, termed *ts*I, such that T_{I} becomes the single transition state (Fig. 3A). Likewise, applying tension in the direction that favors *iso*I (as in junction *XR*) would result in *ts*II becoming the single transition state.

Below, we describe how we determined the ϕ and ψ angles in the transition state from our data. We restrict our discussion to junction *XR* but the same argument applies to junction *HR*. Here, we used a simple geometrical model described in the previous section. For a junction with effective arm length L_{eff}, the distance change between the *iso*I and *iso*II, $\Delta x_{eq} = 2L_{eff}\left(1 - \sin\frac{\phi_0}{2}\right)$ where ϕ_0 is for the stacked-X structure. Using ϕ_0=40° and Δx_{eq}=4.4 nm from the data, we obtain L_{eff}=3.4 nm. We note that this effective length of each arm we deduced is similar to 3.7 nm length calculated by multiplying 11 bp arm length by 0.34 nm of crystallographic base pair length. Since the transition state is in the *iso*II half of the phase space, we need to find $(\phi_{\text{II}}, \psi_{\text{II}})$ such that distance from *iso*II to *ts*II,

$2L_{eff}\left(\sqrt{\cos^2\frac{\psi_{II}}{2}\sin^2\frac{\phi_{II}}{2}+\sin^2\frac{\psi_{II}}{2}}-\sin\frac{\phi_0}{2}\right)$ is equal to $\Delta x_b^{\ddagger}$=1.47 nm. There is a combination of (ϕ_{II}, ψ_{II}) values that satisfy this relation, starting from (70°, 0°) at one extreme and arriving at (0°, 70°) at the other (see figure to the right).

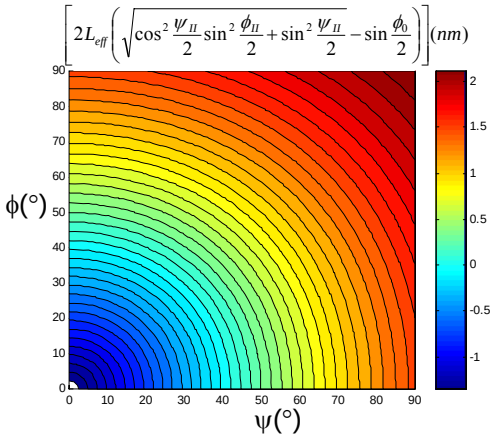

In order to obtain an additional constraint, we measured junction *BR*. This construct gave increase in both forward and backward rates with force. Acceleration in rates with force means that the distance between the two ends of the B and R arm is larger in the transition state than in the stacked-X structures. The distance between the two ends of B and R arms is given by $2L_{eff}\left(\sqrt{\cos^2\frac{\psi_{II}}{2}\cos^2\frac{\phi_{II}}{2}+\sin^2\frac{\psi_{II}}{2}}\right)$ which is relatively insensitive to ψ_{II} for $\phi_{II} < 70°$, and is larger than its value in *iso*II, $2L_{eff}\cos\frac{\phi_0}{2}$, only if $\phi_{II} < \phi_0$. Therefore, the fact that the transition rates increase with force itself already restricts ϕ_{II} to below 40 °. How much below depends on the distance to the transition state. The minimum distance to the transition state we estimated for junction *BR* is 0.37 nm. The equivalent distance in our model is $2L_{eff}\left(\sqrt{\cos^2\frac{\psi_{II}}{2}\cos^2\frac{\phi_{II}}{2}+\sin^2\frac{\psi_{II}}{2}}\right)-2L_{eff}\cos\frac{\phi_0}{2}$ which increases with deceasing ϕ_{II}. Here, it is uncertain which value should be used for L_{eff} because the pulling direction does not define a reaction coordinate that is valid from *iso*I all the way to *iso*II as revealed by a large discrepancy between Δx_{eq} and ($\Delta x_b^{\ddagger} + \Delta x_f^{\ddagger}$) (Table 1). Here, we set L_{eff} to the 11 bp arm length, 3.7 nm. Then, the maximum value of $2L_{eff}\left(\sqrt{\cos^2\frac{\psi_{II}}{2}\cos^2\frac{\phi_{II}}{2}+\sin^2\frac{\psi_{II}}{2}}\right)-2L_{eff}\cos\frac{\phi_0}{2}$ is 0.35 nm when ϕ_{II}=0 (see figure below), and this becomes smaller for smaller L_{eff}. Therefore, in order to account for the

finite distance to the transition state, ϕ_{II} needs to be essentially zero.

Combining results from *XR* and *BR* analysis, we conclude that in the transition state *ts*II, $(\phi_{II}, \psi_{II})_{ts}$=(0°, 70°). This transition state is similar to the open state but with arms veering off by about 20° from the ideal open state. Following the same argument, we can deduce that for the transition state in the *iso*I-like phase space, T_I, has the $(\phi_I, \psi_I)_T$= (0°, 70°) as well.

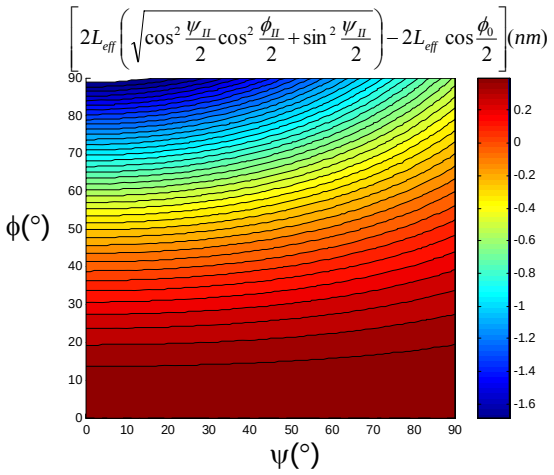

We also note that the equilibrium between the two states does shift with force for junction *BR*. Δx_{eq} is 0.7 nm favoring *iso*I. This value is about 5-6 times lower than those of junctions *XR* and *HR*, confirming our prediction that there will not be as big a change in conformational bias with force for junction *BR*. We suggest that the residual bias we detect here is due to the finite diameter effect of the duplex arms which is amplified for junction BR because two pulling strands are either both exchanging strands (*isoII*) or both continuous strands (*isoI*). The ends of the pulling strands are therefore expected to be farther apart in *isoI* than *isoII* thereby leading to the increased relative population of *isoI* upon force application. Such an effect due to the finite DNA duplex diameter would be much less pronounced in junctions XR and HR because in both conformations, one pulling strand is an exchanging strand and the other is a continous strand.

General comments about the effect of fluorescent labeling and surface tethering on the Holliday junction conformational dynamics.

In the current study, the fluorophores were attached to the DNA at least 11 bp away from the junction core. Likewise, a biotin was attached to the DNA also 11 bp away from the junction core for surface tethering. It is highly unlikely that these modifications and surface tethering could interfere with conformational transitions of the junction as we summarize below.

In previous studies utilizing similar constructs, we have shown that the fluorophore labeling and surface tethering have no effect on the conformational bias by comparing to bulk solution measurements of unlabeled DNA molecules. For example, conformational bias between the two conformers is maintained between single molecule FRET measurements of labeled DNA and gel mobility assay of unlabeled DNA molecules for three different DNA sequences (4,5) and for junctions modified with a methyl phosphonate (6). Furthermore, in a study on branch migration, we showed that conformational bias and branch point bias deduced from single molecule FRET measurements of labeled DNA could be reproduced by a separate chemical probing experiment of unlabeled DNA for four different DNA sequences (7). In addition, magnesium concentration dependence of branch migration rates of the labeled DNA were in agreement with previous gel electrophoresis data of unlabeled DNA reported by Hsieh and colleagues in 1994(8).

In order to test if a particular surface tethering geometry or labeling configuration has any effect on the rates of conformational exchange, we moved the donor and acceptor attachment sites and biotin-attachment sites to different arms of the junction and found identical rates of conformational exchange (5). Even when the organic fluorophore was replaced by a quantum dot as the donor, we found the identical rates of transitions (9). When a second acceptor (Cy5.5) was added to a third arm for three-color FRET experiments so that three fluorophores (Cy3, Cy5, and Cy5.5) are attached to the junction, we still obtained the same rates of conformational transitions (10). The data presented in Fig. S1 show that extending one of the arms by 12 nt of single stranded DNA or lengthening two of the arms by additional 10 bp of double stranded DNA have insignificant effects on the rates of transitions. In summary, all of our previous studies and the current study strongly indicate that fluorescent labeling and surface tethering do not have any significant effect on the Holliday junction conformational dynamics.

SUPPORTING ONLINE FIGURES AND TABLES

Fig. S1. Dynamics of the different Holliday junction structures in their free forms

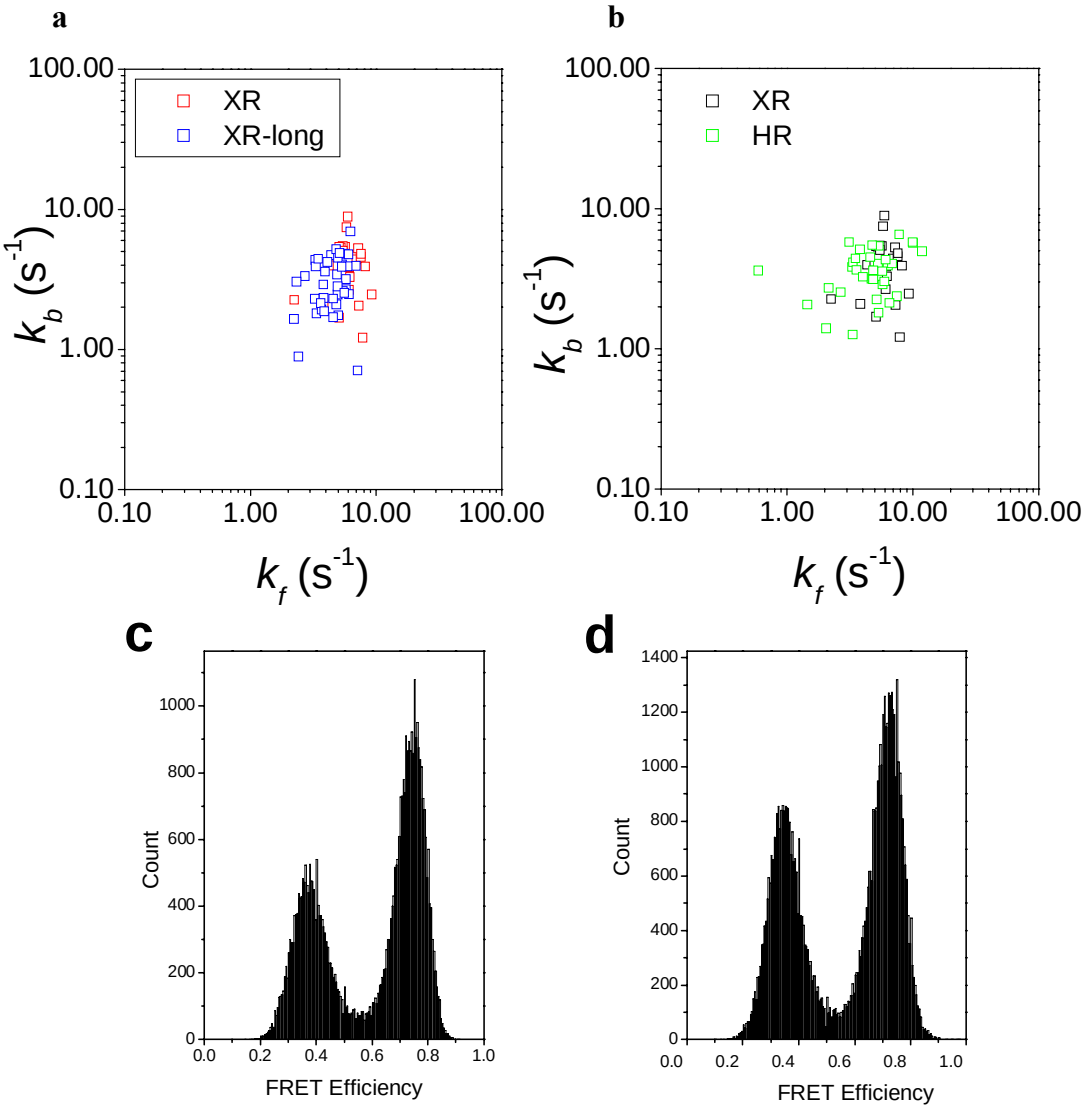

a. Distribution of transition rates of junctions *XR* and *XR*-long. **B**. Distribution of transition rates of junctions *XR* and *HR*. All the data were obtained without a λ-DNA attached in the absence of trapping laser beam, but otherwise in identical solution conditions. **c.** Single molecule FRET efficiency histogram of junction XR (>20 molecules). Each count represents a single data point of 10 ms duration. **d.** Same as **c.** but for junction *HR*.

It is clear from the scatter plots that the dynamic behaviors of the isolated junctions are not modified significantly when the adhesive single stranded tail is added to a different arm and when the arm lengths are changed. There exist significant variations in the transition rates among the nominally identical molecules and such a heterogeneity may be responsible for some variations in the zero force extrapolated rates determined from the force dependence data. For example, in Fig. 2B, zero-force extrapolation would give significantly higher rate for the forward rate. However, Fig. S4 shows a collection of results from five molecules and the data does indicate that the zero-force extrapolation would give on average similar rates for both forward and backward reactions. In Table S2, we summarize the average and standard deviation of the rates for the isolated junctions and for the junctions under force that yielded the zero-force extrapolated rates. Importantly, they show that lengthening of X and R arms (XR-long) by about a factor of two changes the conformational exchange rates of free junctions by only about 25% which is similar to the variations between individual molecules of each construct and is also similar to the difference between junctions XR and HR. Therefore, it is likely that the proximity of the junction core to the surface does not influence the junction dynamics significantly for arms at least 11 bp long.

Table S2. Comparing the transitions rates for zero-force extrapolation and for free forms of the junctions.

	XR	*XR*-long	*HR*
k_b (s^{-1}) free junction	4.2±1.9	3.2±1.3	3.7±1.3
k_f (s^{-1}) free junction	6.1±1.6	4.6±1.2	5.0±2.4
k_b (s^{-1}) zero force	11±2.7	16±4.5	18±1.3
k_f (s^{-1}) zero force	9.9±3.3	16±2.5	11±1.9

These results show that the zero force extrapolation yields rates that are 3 to 4 times higher for the forward reaction and 1.5 to 3.5 times higher for the backward reaction. To test if a temperature increase due to the trapping laser may be responsible for the increase in rates, we measured the isolated junction *XR* molecules with and without the trapping laser focused 13 μm from the junction. The result is summarized below in Table S3.

Table S3. Comparing the transitions rates for zero-force extrapolation and for free forms of the junctions.

	XR (free junction, no trapping laser)	*XR* (free junction, trapping laser on)
k_b (s^{-1})	4.7±1.4	6.2±1.9
k_f (s^{-1})	7.2±4.2	11.3±4.8

As can be seen in Table S3, heating effect can explain the rate increases of up to 1.5 fold in both forward and backward reactions. Since the enthalpic barrier determined from temperature dependent studies of the junction of same sequence was 110 kJ/mole (4), 50% increase in rate corresponds to about 2-3° C increase in temperature induced by the trapping laser. The remaining differences (~ 2 fold) may have multiple origins, for example, (1) λ-DNA may tug on the junction continually even in the absence of applied force, (2) λ-DNA may alter the electrostatic environment of the junction. We note that the conformer transition rate can vary by more than two orders of magnitude when the ionic conditions are changed (5). The relatively good agreement between the free junction data and the extrapolation of the force-dependent data suggest that the reaction mechanism is not significantly altered by the application of force.

Fig. S4. Comparing conformer exchange rates vs. force between junctions XR and XR-long

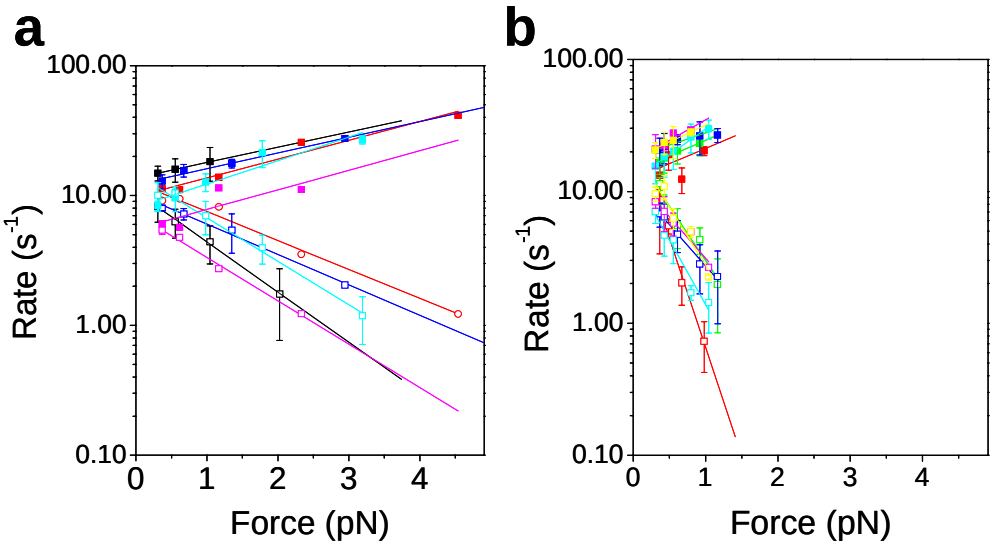

a. Rate constants of conformer exchange vs. force for 5 different *XR* molecules. Different molecule are differentiated by colors. Backward reaction rates from *isoII* to *isoI* were represented as solid data point and forward rates from *isoI* to *isoII* as open data points. Linear fits are also shown. When the force dependence measurements were made more than once because photobleaching did not terminate the experiment after one force cycle, error bars are added representing the standard deviation between different sets. **b.** Same as in **a** but for *XR*-long molecules. It is clear that *XR*-long exhibits much greater changes in rates for the same range of force.

Fig. S5. A schematic of optical setup

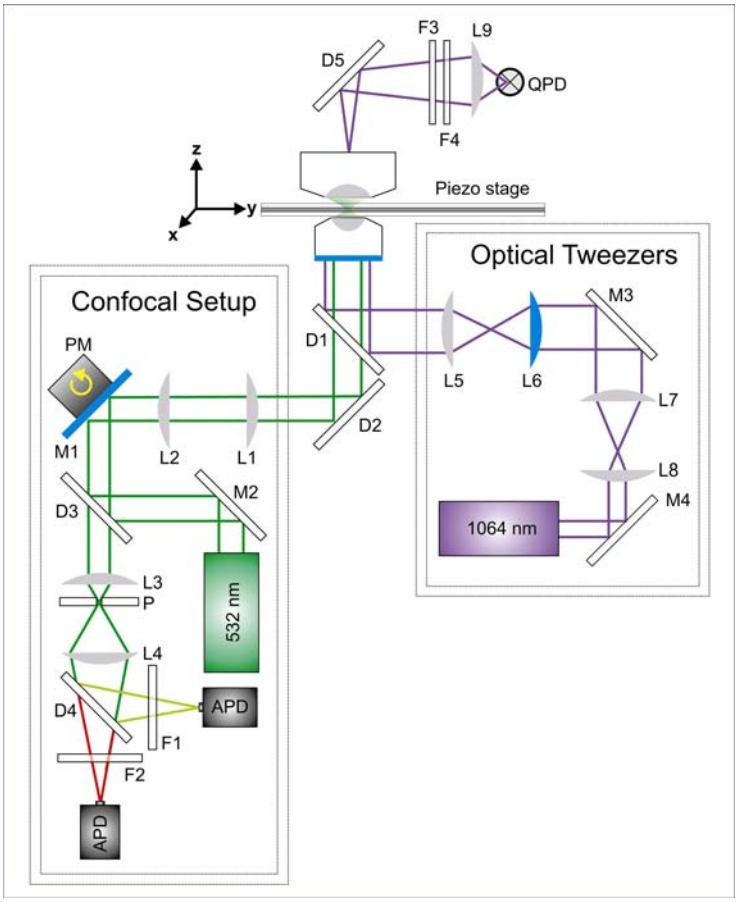

The optical tweezers and single-molecule confocal fluorescence setup were built on a commercial inverted microscope (IX71, Olympus) equipped with a three-dimensional piezo stage (Physik Instruments). The trapping laser (1064 nm, 1 W, CrystaLaser) was coupled through the back port and guided to the sample space through the oil-immersion objective (100x/1.40, Olympus) to trap a bead, and then to the quadrant photodiode (UDT SPOT/9DMI) through the condenser to detect the deviation of the trapped bead position from the trap center. Excitation laser (532 nm, 30 mW, World StarTech) was coupled through the right side port. The fluorescence emission was also collected through the same port. Two telescopic lenses (L1 and L2) were positioned to get uniform excitation independent on incidence angle of the excitation beam scanned by a piezo-controlled mirror mount (S-334K010, Physik Instrument) which has two degree of freedom. Optical path below the dichroic, D3, does not depend on the incidence angle of the green laser. The

abbreviations used for the optical components in the figure are: M, mirror; L, lens; D, dichroic; F, filter; QPD, quadrant photodiode; PM, piezo-controlled mirror mount; P, pinhole; APD, avalanche photodiode.

The voltage signals from the QPD were converted to x and y positions of a bead stuck in the same plane by raster-scanning the sample and measuring the voltage signals. The mapping was obtained using a fifth order polynomial fit as described previously (11). The trap stiffness of 0.11 pN/nm was obtained by fitting the power spectrum (sampling rate of 10 kHz) of position signal of a trapped bead using a Lorenzian function, and accounting for the hydrodynamic correction (12). The trapping laser power just before it entered the microscope was 900 mW.

At 2 pN of force and at 100 Hz bandwidth (same as what was used for FRET detection), our optical trap instrument has the force detection noise of 0.2 pN, corresponding to the bead's displacement noise of □ 2 nm. The effective stiffness of the lambda DNA used in this study at 2 pN of force is about 0.002 pN/nm, estimated using the worm like chain model. Therefore, the junction's movement by up to about 5 nm upon conformational exchange would result in 0.01 pN of additional force fluctuation of the trapped bead which is much smaller than the applied force and the force detection noise. As a consequence, our instrument operates effectively as a constant force apparatus and the Holliday junction's conformational fluctuations can not be detected via force measurements. This is in contrast to previous higher resolution studies of DNA unzipping that used 50 times shorter DNA at forces higher than 10 pN, in which the effective stiffness of the DNA is > 1.5 pN/nm so that the stiffness of the trap is what matters. In such a case, 5 nm movement would result in 0.5 pN of force change, necessitating active force clamping.

Fig. S6. Calibration of piezo-controlled mirror

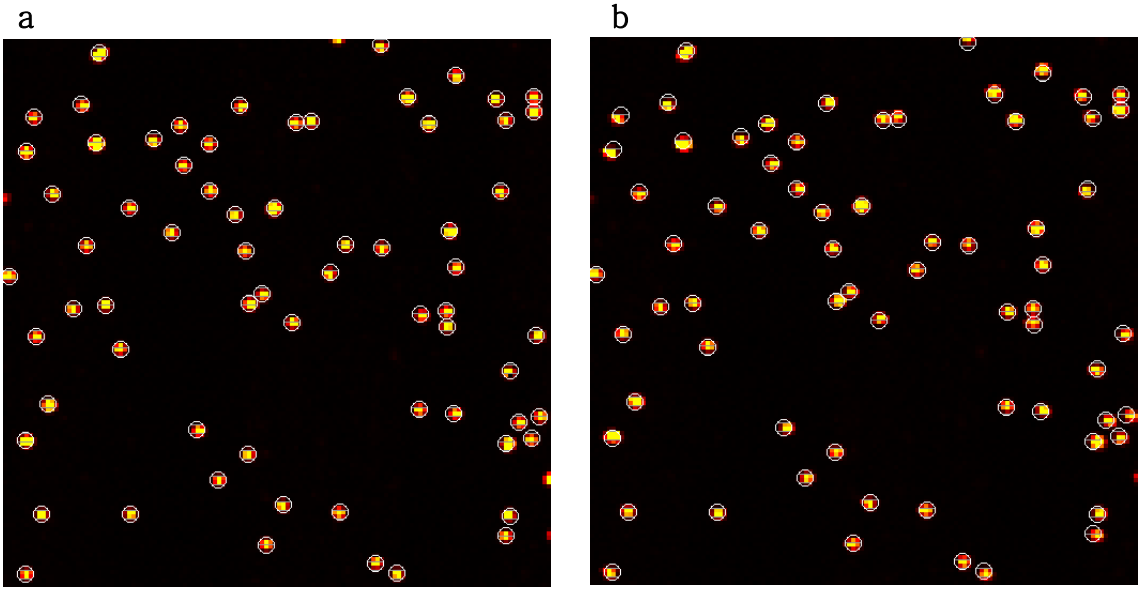

A fluorescent bead sample was used to create a mapping between the piezo-controlled mirror deflection angle and the resulting nm displacement in the sample plane. **a.** First the bead sample was imaged by fixing the confocal spot while scanning the piezo stage (scan area, 38.4 μm x 38.4 μm). This image was mapped to. a second image (**b**) that was formed by scanning the confocal spot through an angular scan of the piezo mirror while the stage remained stationary. We used 3rd order polynomial fit to a calibration file which was then used to map a sample plane position to a corresponding angle of the piezo mirror. Using this mapping, we were able to synchronize the movement of the sample stage with the tilting of the mirror such that the confocal excitation beam keeps track of the DNA junction under investigation when the junction position is changed to achieve the desired force.

References

1. Ha, T., Rasnik, I., Cheng, W., Babcock, H. P., Gauss, G., Lohman, T. M., and Chu, S. (2002) *Nature* **419**, 638-641
2. Rasnik, I., McKinney, S. A., and Ha, T. (2006) *Nat Methods* **3**, 891-893
3. McKinney, S. A., Joo, C., and Ha, T. (2006) *Biophys J* **91**, 1941-1951

4. McKinney, S. A., Declais, A. C., Lilley, D. M. J., and Ha, T. (2003) *Nature Structural Biology* **10**, 93-97
5. Joo, C., McKinney, S. A., Lilley, D. M. J., and Ha, T. (2004) *J Mol Biol* **341**, 739-751
6. Liu, J., Declais, A. C., McKinney, S. A., Ha, T., Norman, D. G., and Lilley, D. M. (2005) *Chem Biol* **12**, 217-228
7. McKinney, S. A., Freeman, A. D., Lilley, D. M., and Ha, T. (2005) *Proc Natl Acad Sci U S A* **102**, 5715-5720
8. Panyutin, I. G., and Hsieh, P. (1994) *Proceedings of the National Academy of Sciences of the United States of America* **91**, 2021-2025
9. Hohng, S., and Ha, T. (2005) *Chemphyschem* **6**, 956-960
10. Hohng, S., Joo, C., and Ha, T. (2004) *Biophys J* **87**, 1328-1337
11. Lang, M. J., Asbury, C. L., Shaevitz, J. W., and Block, S. M. (2002) *Biophys J* **83**, 491-501
12. Hagedorn, P. H., Flyvbjerg, H., and Moller, I. M. (2004) *Physiol Plant* **120**, 370-385